Wideband Multi-polarization Reconfigurable Antenna based on Non-uniform Polarization Convert AMC Reflector

Long Li[1], Jia-Jun Liang[1,2], Xiaoxiao Liu[3], Tiejun Chen[2], Jier Lv[1], and Zhao Wu[1,2*]

[1]Research Center of Intelligent Information and Communication Technology

[2]Guangxi Colleges and Universities Key Lab of Complex System Optimization and Big Data Processing
Yulin Normal University, Yulin 537000, China
longli@ylu.edu.cn, shuigpjd@163.com, chentj@ylu.edu.cn, jielv@ylu.edu.cn, kianty@163.com*

[3]Wuhan Maritime Communication Research Institute
Wuhan 430000, China.
xxliu1215@163.com

Abstract **–** A novel design of wideband multi-polarization reconfigurable antenna is proposed, based on a non-uniform polarization convert artificial magnetic conductor (AMC) reflector. The proposed antenna consists of a radiator element and an AMC reflector. Firstly, a modified polarization convert AMC reflector is designed. The non-uniform AMC reflector causes an enhancement of 3 dB axial ratio (AR) performance. Secondly, a wideband linearly polarized monopole antenna is presented as the main radiator, utilizing the broadband characteristic of a C-shaped monopole. The polarization reconfigurability of the proposed antenna can be achieved by properly rotating the AMC reflector, which can be switched between linear polarization (LP), left-hand circular polarization (LHCP), and right-hand circular polarization (RHCP). A prototype of the proposed antenna is fabricated and experimented with to validate the theoretical performance. The measured results show a -10 dB impedance bandwidth of 42.7% and 44.4% for LP and CP modes, respectively, and a 3 dB AR bandwidth of 20% for CP modes. In addition, the measured peak gain reaches 8 dBi/dBic. A good agreement is shown between the simulation and measurement, pointing to the good performance of the proposed antenna.

Index Terms **–** Non-uniform metasurface (MS), polarization convert AMC reflector, polarization reconfigurability, wideband.

I. INTRODUCTION

With the rapid development of mobile and satellite communications, lots of multifunctional antennas have been investigated in recent years, such as frequency reconfigurable antennas, pattern reconfigurable antennas, polarization reconfigurable antennas, or hybrid reconfigurable antennas [1]–[25]. Since circular polarization has the characteristic of reducing the effect of multipath loss, modern wireless communications require antenna polarization diversity to strengthen the communication quality, especially for satellite communications [3], [4]. Moreover, to meet more wireless communication applications needs, a wideband characteristic of the antenna is needed. Thus, the antenna, which combines performances of wideband and multi-polarization simultaneously, has attracted more and more attention.

Conventionally, the approach of antenna reconfigurability includes embedding RF or optical switches in slots on radiator patches or the ground plane to change the antenna current distribution and make different polarization modes [5]–[14]. In [5]–[7], three tri-polarization reconfigurable patch antennas are presented; they have simple geometries, but all obtain a narrow operating bandwidth of 2%, 8%, and 3%, respectively. On the contrary, a tri-reconfigurable antenna makes a large 3 dB axial ratio (AR) bandwidth of 50% caused by a C-shaped radiator [8], but the optical switch is not easy to apply to modern communication systems. Some other works unfortunately have polarization reconfigurability, switching only within linearly polarized (LP) modes or circularly polarized (CP) modes [9]–[12]. Other works realize polarization diversity by controlling switches inserted in the slot on the ground plane [13], [14].

Another method for a polarization reconfigurable antenna is to design a multipath phase-shift network, which can change the phase difference between the feeding points and lead to polarization diversities [15]–[10]. In this method, it is easy to offer a phase difference and then achieve polarization diversity. For example, in [15] and [18], a tri-polarization reconfigurable antenna and a quad-polarization reconfigurable antenna are proposed,

Submitted On: February 1, 2023
Accepted On: June 25, 2023

https://doi.org/10.13052/2023.ACES.J.380909

but they obtain a narrow 3 dB AR bandwidth of 17% and 12%, respectively. Obviously, the shortcoming of this method is that a wideband phase-shift network is challenging to implement, and many lumped components are used, which causes cost increases.

It's worth noting that, as a novel design, some multi-polarization antenna investigations about metasurface (MS) for polarization diversity have been presented [20]–[25]. Compared with conventional works, the polarization reconfigurable antenna based on MS has the advantage of a low profile. In [20], a CP reconfigurable antenna based on non-uniform MS with a low profile and broadband is investigated, controlled by RF switches. Unfortunately, this antenna can't work in LP mode. In [23], a multi-polarization reconfigurable antenna based on polarization convert MS is proposed with a bandwidth of 30%, switching polarization states by rotating the MS. Compared with RF switches, this method can reduce the loss of bias circuits and lumped components.

In this paper, a wideband multi-polarization reconfigurable antenna based on a polarization convert artificial magnetic conductor (AMC) reflector is proposed. Different from the previously published design, this antenna is beneficial for a simple polarization switching strategy and a reduction of loss, selecting polarization modes by properly rotating the AMC reflector without any switches. Meanwhile, compared to the conventional metal reflector, the AMC reflector leads to an improvement of the antenna gain with a low profile. Eventually, the proposed antenna acquires multi-polarization working modes and a profile decline of 33.3% compared to conventional mental reflectors with a profile of $1/4\lambda 0$ (at $f0 = 5$ GHz).

II. ANTENNA DESIGN PRINCIPLE

As depicted in Fig. 1, the proposed antenna includes an AMC reflector and a C-shaped radiator. The wideband performance of the C-shaped radiator has already been validated by previous work [8]. There is a modified C-shaped monopole to offer a wideband incident wave source. The modified C-shaped patch and ground plane are printed on top and bottom of a 1.524 mm Rogers 4003C substrate with a relative permittivity of 3.38. In others, an improved AMC reflector is placed $H = 10$ mm below the radiator to achieve polarization reconfigurability and radiation directionality. The AMC reflector consists of 6×6 MS units fabricated on a 2 mm R4 substrate with a relative permittivity of 4.4. To explain the design principle of the proposed antenna, a detailed analysis of the AMC reflector and C-shaped monopole are discussed as follows.

A. Polarization convert AMC reflector analysis

The geometry of the proposed AMC unit is illustrated in Fig. 2, in which its cell is a shuttle-shaped patch etched with a crossed slot. An equivalent circuit is provided to explain how the AMC reflector realizes polarization conversion. Along the diagonal corners, the orthogonal surface impedance component, marked Z_u and Z_v, of the AMC unit can be approximately calculated as

$$\begin{aligned} Z_u &= 2R_1 + 2j\omega(2L_1) + 2/(j\omega C_1) \\ &\quad + 1/(j\omega C_2) \\ &= R_u + jX_u \text{ and} \end{aligned} \tag{1a}$$

$$\begin{aligned} Z_v &= 2R_2 + 2j\omega(2L_2) + 2/(j\omega C_3) \\ &\quad + 1/(j\omega C_4) \\ &= R_v + jX_v, \end{aligned} \tag{1b}$$

where $R1$, $L1$, $C1$, and $C2$, are the resistance, inductance, and distributed capacitance of the AMC unit in the u-direction, respectively, and $R2$, $L2$, $C3$, and C4 are in the v-direction. Further, according to the Euler formula, (1) can be simplified as follows

$$Z_u = |Z_u|\angle\varphi 1 = |Z_u|e^{j\varphi 1} \text{ and} \tag{2a}$$

$$Z_v = |Z_v|\angle\varphi 2 = |Z_v|e^{j\varphi 2}. \tag{2b}$$

What can be known is that the resistance, inductance, and distributed capacitance of the AMC unit are related to the triangle truncation and the crossed slot. Thus, by adjusting the size of the triangle truncated and the crossed slot, a phase difference can be achieved between Z_u and Z_v.

Assuming that the incident source is a linearly polarized plane wave along the x-axis, so the incident $\boldsymbol{E}$-field is also along the x-axis named $\boldsymbol{E}_{ix}$. Here, $\boldsymbol{E}_{ix}$ is broken into two orthogonal components, $\boldsymbol{E}_{iu}$ and $\boldsymbol{E}_{iv}$. By supposing that the magnitude of the two orthogonal $\boldsymbol{E}$-field

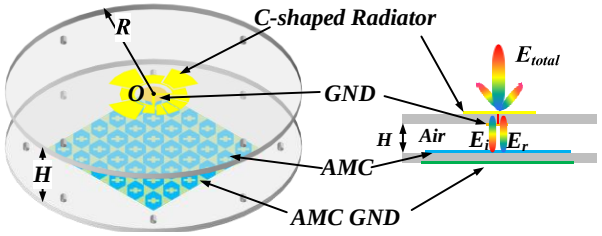

Fig. 1. The overall prototype of the proposed antenna.

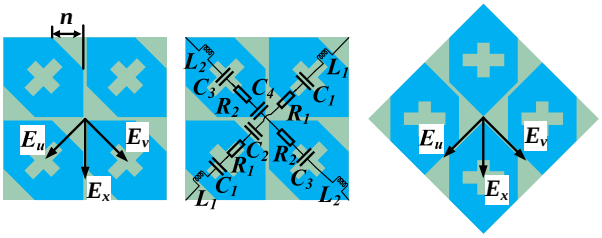

Fig. 2. The geometry of the proposed AMC.

components is $|E_m|$ and the phase is $\ddot{o}3$ and $\ddot{o}4$, $\boldsymbol{E}_{iu}$ and $\boldsymbol{E}_{iv}$ can be denoted by the following:

$$E_{\text{iu}} = |Zm|e^{j\varphi 3} \text{ and} \tag{3a}$$

$$E_{\text{iv}} = |Zm|e^{j\varphi 4}. \tag{3b}$$

When $\boldsymbol{E}$-field components $\boldsymbol{E}_{iu}$ and $\boldsymbol{E}_{iv}$ are incident on the AMC reflector, respectively, numerous electrons on the surface of the AMC unit will be excited and move along the u-direction and v-direction, respectively, generating induced currents, thus forming the reflected $\boldsymbol{E}$-fields $\boldsymbol{E}_{ru}$ and $\boldsymbol{E}_{rv}$ individually. If there is no energy loss in reflection, the reflected and incident $\boldsymbol{E}$-field are equal in magnitude. Furthermore, the phase of the reflected wave is equivalent to the combination of the phase with the incident wave, the phase of the AMC surface impedance along the incident wave direction, and the phase difference generated by the air gap. Therefore, the reflected $\boldsymbol{E}$-field components can be roughly described as follows

$$E_{ru} = |Zm|e^{j(\varphi 1+\varphi 3+\Delta\varphi)} \text{ and} \tag{4a}$$

$$E_{rv} = |Zm|e^{j(\varphi 2+\varphi 4+\Delta\varphi).} \tag{4b}$$

Eventually, the composite $\boldsymbol{E}$-field components can be roughly described as follows:

$$E_u = |Zm|\left[e^{j\varphi 3} + e^{j(\varphi 1+\varphi 3+\Delta\varphi)}\right] \text{ and} \tag{5a}$$

$$E_v = |Zm|\left[e^{j\varphi 4} + e^{j(\varphi 2+\varphi 4+\Delta\varphi)}\right]. \tag{5b}$$

Since $\boldsymbol{E}_{iu}$ and $\boldsymbol{E}_{iv}$ are symmetric to $\boldsymbol{E}_{ix}$, these two orthogonal $\boldsymbol{E}$-field components have the same phase, meaning that $\ddot{o}3$ is equal to $\ddot{o}4$. And appropriately optimizing the AMC unit, a 90° phase difference can be obtained between Z_u and Z_v, assuming $\ddot{o}1$ leads $\ddot{o}2$ by 90°. As a result, (5a) and (5b) can be simplified as (6a) and (6b).

$$E_u = |Zm|\left[e^{j\varphi 4} + je^{j(\varphi 2+\varphi 4+\Delta\varphi)}\right] \text{ and} \tag{6a}$$

$$E_v = |Zm|\left[e^{j\varphi 4} + e^{j(\varphi 2+\varphi 4+\Delta\varphi)}\right]. \tag{6b}$$

Thus, the composite $\boldsymbol{E}$-field $\boldsymbol{E}_{total}$ is a CP wave, which is combined by two $\boldsymbol{E}$-field components with identical magnitudes and a 90° phase difference. In addition, because the phase of the $\boldsymbol{E}$-field component in the u-direction leads the v-direction, the antenna will work in left-handed circularly polarized (LHCP) mode. As shown in Fig. 2, when the AMC unit is rotated by -45° or 45°, the AMC is symmetric about the x-axis. Thus, there is an in-phase or anti-phase of the surface impedance between the u-direction and v-direction. Accordingly, the composite $\boldsymbol{E}$-field $\boldsymbol{E}_{total}$ is an LP wave. Moreover, when the AMC unit is rotated by 90°, the polarization of the proposed antenna will be in right-handed circularly polarized (RHCP) mode.

Ansoft HFSS simulates the AMC unit with the Floquet port to verify the analysis. The width of the triangle truncation on AMC units is defined as parameter n. Its effect on the reflected characteristic of the proposed AMC unit and the polarization convert performance is given in Fig. 3. With the increase of n, the high-frequency resonance point of the AMC unit will move toward the high frequency, whereas the low frequency remains almost constant. Meanwhile, the impedance matching would deteriorate. In addition, for better CP performance, the magnitude ratio between the incident $\boldsymbol{E}$-field and the reflected must be within ±3 dB. As shown in Fig. 3 (b), while n increases, the magnitude ratio varies, and the broadest 3 dB magnitude ratio bandwidth is obtained when n is equal to 6 mm. Considering the performance of the impedance matching and the CP, there are two AMC units with different truncations, n = 4.5 mm and 6 mm, respectively, to build a non-uniform AMC reflector.

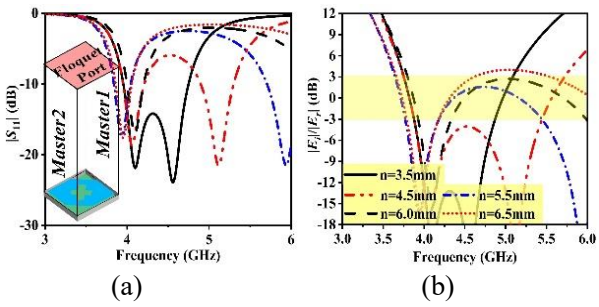

(a) (b)

Fig. 3. The effect of parameter n on the AMC unit: (a) Reflection coefficient $|S_{11}|$, (b) the magnitude ratio between the incident E-field and reflected E-field.

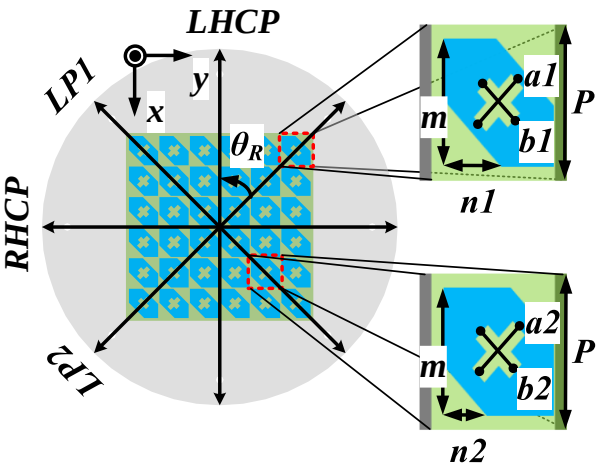

Fig. 4. The phototype of the proposed AMC reflector (design parameters: m = 11.5 mm, P = 12 mm, $n1$ = 6 mm, $n2$ = 4.5 mm, $a1$ = 5.5 mm, $a2$ = 6 mm, $b1$ = 4.5 mm, $b2$ = 5 mm).

B. C-shaped monopole antenna with the AMC reflector

Given the polarization conversion characteristic of the proposed AMC reflector, a modified C-shaped monopole is designed and introduced to offer an incident *x*-LP wave source, positioned at the top of the reflector.

As shown in Fig. 5, for Ant. 1, the impedance matching is poor, in which the real part of the impedance is not close to 50 Ù, and the imaginary part is not near 0 Ù within a certain bandwidth. There is a resonance only near 4 GHz, noted f_1. To improve impedance matching and bring multi-resonance, the C-shaped patch edge is slotted and placed into three parasitic stubs in a fan shape, labeled Ant. 2. Due to the slotting, the current length of the resonant frequency f_1 will be expanded so that the resonance frequency is scaled down and recorded as f_2. The parasitic stubs, with the induced current, will create a new resonance, marked f_3, achieving multi-frequency resonance. As a result, two resonant frequency points near 3 and 5 GHz are generated and bring a wide impedance bandwidth ($|S_{11}| <$ -10 dB) of about 60%.

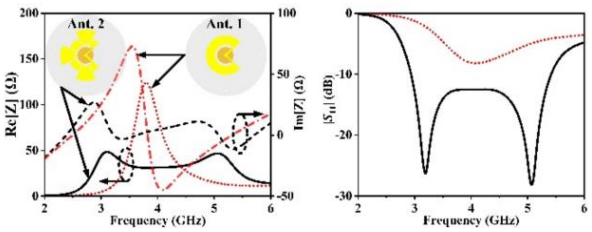

(a) (b)

Fig. 5. The performance of two C-shaped monopoles: (a) Impedance, (b) $|S_{11}|$.

Then the proposed AMC reflector is applied below the C-shaped monopole antenna, about 0.15ë, to realize directionality and polarization reconfigurability. To reduce the crossed polarization, especially in CP modes, a set of fan-shaped parasitic stubs are added at the notch of Ant.2. The added parasitic stubs will be excited and generated with a polarization mode consistent with the antenna, so the main polarization is enhanced, which implies a reverse weakening of the cross-polarization, as shown in Fig. 6. The final design of the C-shaped monopole antenna, shown in Fig. 7, contains a C-shaped patch with seven parasitic fan stubs and a circular ground plane with two additional rectangle stubs.

Eventually, when holding the C-shaped monopole antenna still and rotating the AMC reflector counterclockwise by -45°, 45°, 0°, and 90°, the antenna can work on *x*-LP1, *x*-LP2, LHCP, and RHCP modes, respectively.

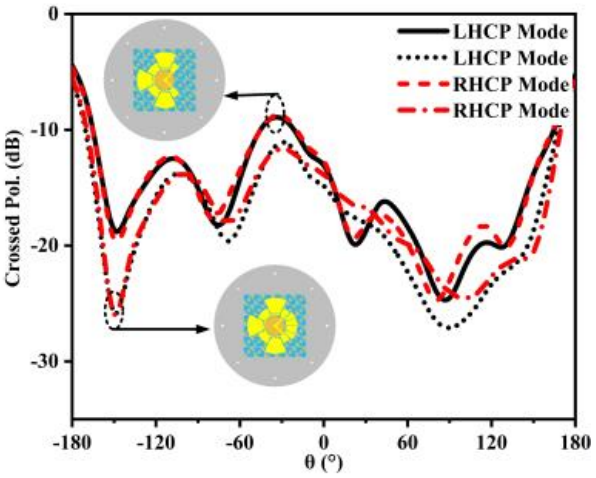

Fig. 6. The effect of the small fan parasitic stubs.

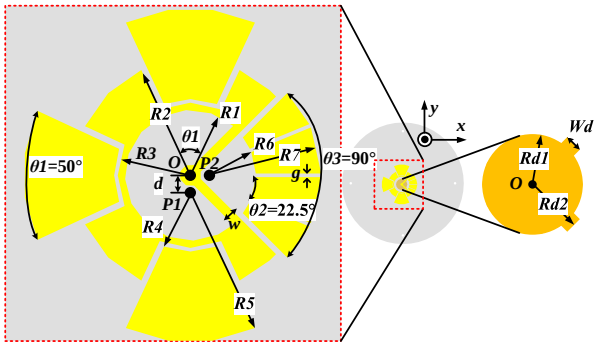

Fig. 7. The phototype of the C-shaped monopole (design parameters [millimetres]: *R1* = 9, *R2* = 16, *R3* = 10, *R4* = 8.5, *R5* = 21, *R6* = 7, *R7* = 16, *Rd1* = 6.5, *Rd2* = 7.5, *w* = 1.3, *d* = 2, *g* = 0.5, *Wd* = 2.3).

III. SIMULATED AND EXPERIMENTAL RESULTS

The proposed antenna is designed and optimized by Ansys HFSS and then fabricated and measured to verify the performance by the ROHDE&SCHWARZ ZVB-8 vector network analyzer and multi-probe antenna testing system. The manufactured antenna and far-field experiment setup are shown in Fig. 8.

Figure 9 illustrates simulated and experimental reflection coefficients $|S_{11}|$ in different polarization modes. The experimental -10 dB overlapped impedance bandwidth of 42.7%, covers 3.5 GHz to 5.4 GHz in both LP modes. It obtains 44.4% of the measured -10 dB impedance bandwidth for the CP modes and covers between 3.5 GHz and 5.5 GHz. The measured impedance matching of the antenna decreases slightly at high frequency due to manufacturing error. The experimental results are in good accordance with the simulation results.

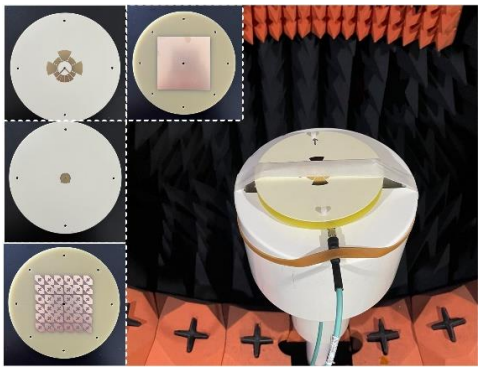

Fig. 8. Photographs of the manufactured antenna and experiment setup.

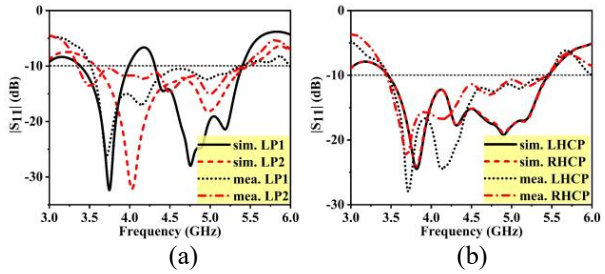

Fig. 9. The simulated and measured reflection coefficient $|S_{11}|$: (a) LP modes and (b) CP modes.

Figure 10 shows the simulated and measured axial ratio and gain in different polarization modes. When working in LP modes, the axial ratio of the antenna is larger than 25 dB within operating bandwidth. In addition, the measured peak gain reaches about 8 dBi. When working in CP modes, an overlapped 3 dB axial ratio bandwidth of 20%, covering 4.5 GHz to 5.5 GHz, shows good agreement with the simulation. Similarly, the measured peak gain is about 8 dBic for CP modes. Compared with the simulations, there is a 2 dB loss of the measured gain, which is caused by the error of fabrication and the loss of dielectric material. The measured and simulated normalized radiation patterns of the proposed antenna at

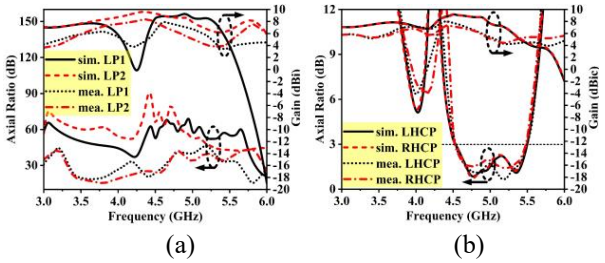

Fig. 10. The simulated and measured results of axial ratio and gain: (a) LP modes and (b) CP modes.

4.8 and 5 GHz are illustrated in Figs. 11 and 12 for CP and LP modes, respectively. The simulated results match well for all states with good directivity.

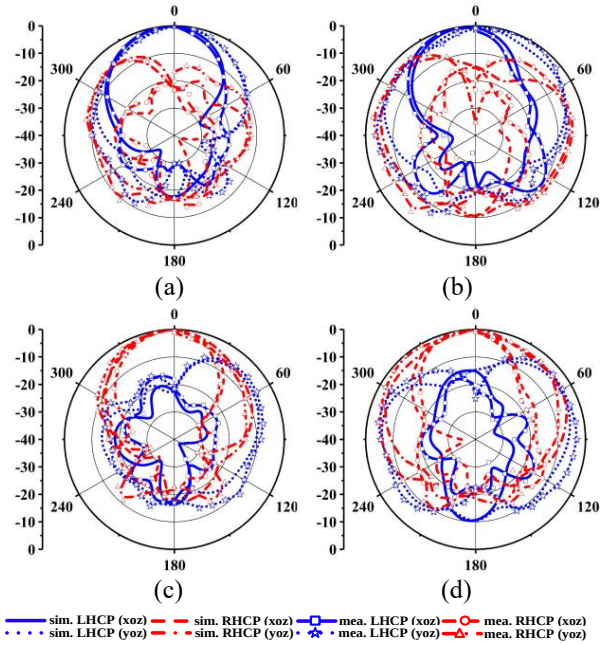

Fig. 11. The simulated and measured normalized radiation pattern: (a) LHCP at 4.8 GHz, (b) 5.2 GHz, (c) RHCP at 4.8 GHz, and (d) 5.2 GHz.

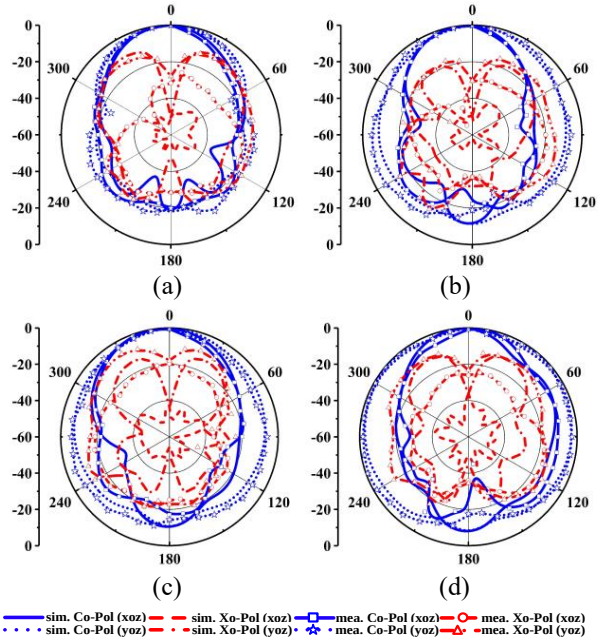

Fig. 12. The simulated and measured normalized radiation pattern: (a) LP1 at 4.8 GHz, (b) 5.2 GHz, (c) LP2 at 4.8 GHz, and (d) 5.2 GHz.

Table 1 shows a performance comparison with other polarization reconfigurable works. The proposed antenna has a wider -10 dB impedance bandwidth of over 40% and more operating modes. Meanwhile, this work has a simple polarization switch strategy by rotating the MS, with no RF switches applied. In addition, the 3 dB axial ratio bandwidth and peak gain of the proposed work have shown good performance.

Table 1: Performance comparison with other works

Ref.	Modes	Impedance Bandwidth (%)	AR Bandwidth (%)	Peak Gain (dBi/c)
[11]	2 CP	41.1	34	12
[12]	2 CP	5	4	5.2
[21]	2 CP	36	21.5	15.5
[22]	1 LP2 CP	LP: 17.1 CP: 8.7	8.7	LP: 9 CP: 8.3
This work	2 LP2 CP	LP: 42.7 CP: 44.4	20	LP: 8 CP: 8

IV. CONCLUSION

This paper proposes a design for a polarization reconfigurable antenna based on a rotating AMC reflector. The proposed antenna is composed of two parts, an AMC reflector and a C-shaped monopole. By turning the AMC reflector at $\pm 45^\circ$, 0°, and 90° clockwise, respectively, the antenna could switch the polarization state among x-LP, LHCP, and RHCP. Compared to other previous polarization reconfigurable antennas, it reduces the application of the DC bias circuits with a simple polarization switching strategy. The proposed antenna has a wide operating bandwidth of 42.7% and 20% for LP and CP modes, approximately covering 3.5 to 5.4 GHz and 4.5 to 5.5 GHz, respectively. Furthermore, the maximum measured gain reaches 8 dBi(c). It could be applied to 5G mobile communication systems, satellite communications, and other polarization-diverse applications.

ACKNOWLEDGMENT

This work was supported in part by the Natural Science Foundation Fund Project in Guangxi, China, under Grant 2021GXNSFBA220003, in part by General Project of Guangxi Natural Science Foundation Project (Guangdong-Guangxi Joint Fund Project) 2021GXNSFAA075031.

REFERENCES

[1] R. L. Haupt and M. Lanagan, "Reconfigurable antennas," *IEEE Antennas and Propagation Magazine*, vol. 55, no. 1, pp. 49-61, Feb. 2013.

[2] K. Ramahatla, M. Mosalaosi, A. Yahya, and B. Basutli, "Multiband reconfigurable antennas for 5G wireless and CubeSat applications: A review," *IEEE Access*, vol. 10, pp. 40910-40931, 2022.

[3] W. Yang, W. Che, H. Jin, W. Feng, and Q. Xue, "A polarization-reconfigurable dipole antenna using polarization rotation AMC structure," *IEEE Transactions on Antennas and Propagation*, vol. 63, no. 12, pp. 5305-5315, Dec. 2015.

[4] B. S. Qiu, Y. F. Xia, and Y. S. Li, "Gain-enhanced wideband circularly polarized antenna with a non-uniform metamaterial reflector," *Applied Computational Electromagnetics Society (ACES) Journal*, vol. 37, no. 3, pp. 281-286, Mar. 2022.

[5] R. K. Singh, A. Basu, and S. K. Koul, "A novel reconfigurable microstrip patch antenna with polarization agility in two switchable frequency bands," *IEEE Transactions on Antennas and Propagation*, vol. 66, no. 10, pp. 5608-5613, Oct. 2018.

[6] S. G. Zhou, G. L. Huang, H.-Y. Liu, A. S. Lin, and C. Y. D. Sim, "A CPW-fed square-ring slot antenna with reconfigurable polarization," *IEEE Access*, vol. 6, pp. 16474-16483, 2018.

[7] Q. Chen, J. Y. Li, G. Yang, B. Cao, and Z. Zhang, "A polarization-reconfigurable high-gain microstrip antenna," *IEEE Transactions on Antennas and Propagation*, vol. 67, no. 5, pp. 3461-3466, May 2019.

[8] G. Jin, L. Li, W. Wang, and S. W. Liao, "A wideband polarization reconfigurable antenna based on optical switches and C-shaped radiator," *Microwave Optical Technology Lett.*, vol. 22, pp. 2415-2422, 2020.

[9] A. Bhattacharjee and S. Dwari, "A monopole antenna with reconfigurable circular polarization and pattern tilting ability in two switchable wide frequency bands," *IEEE Antennas and Wireless Propagation Letters*, vol. 20, no. 9, pp. 1661-1665, Sep. 2021.

[10] K. D. Hong, X. Chen, X. Zhang, L. Zhu, and T. Yuan, "A slot-loaded high-gain circular patch antenna with reconfigurable orthogonal polarizations and low cross polarization," *IEEE Antennas and Wireless Propagation Letters,* vol. 21, no. 3, pp. 511-515, Mar. 2022.

[11] Q. C. Ye, J. L. Li, and Y. M. Zhang, "A circular polarization-reconfigurable antenna with enhanced axial ratio bandwidth," *IEEE Antennas and Wireless Propagation Letters*, vol. 21, no. 6, pp. 1248-1252, June 2022.

[12] A. Priya, S. K. Mohideen, and M. Saravanan, "Design of polarization reconfigurable patch antenna for wireless communications," *Applied Computational Electromagnetics Society (ACES) Journal*, vol. 35, no. 8, pp. 893-898, Aug. 2020.

[13] W. W. Yang, X. Y. Dong, W. J. Sun, and J. X. Chen, "Polarization reconfigurable broadband dielectric resonator antenna with a lattice structure," *IEEE Access,* vol. 6, pp. 21212-21219, 2018.

[14] M. Li, Z. Zhang, M. C. Tang, L. Zhu, and N. W. Liu, "Bandwidth enhancement and size reduction of a low-profile polarization-reconfigurable antenna by utilizing multiple resonances," *IEEE Transactions on Antennas and Propagation*, vol. 70, no. 2, pp. 1517-1522, Feb. 2022.

[15] W. Sun, S. Liu, X. Zhu, X. Zhang, P. L. Chi, and T. Yang, "A novel 1.05 GHz to 1.25 GHz filtering antenna feeding network with reconfigurable frequency and polarization," *IEEE Transactions on Antennas and Propagation*, vol. 70, no. 1, pp. 156-166, Jan. 2022.

[16] C. Liu, Y. Li, T. Liu, Y. Han, J. Wang, and S. Qu, "Polarization reconfigurable and beam-switchable array antenna using switchable feed network," *IEEE Access*, vol. 10, pp. 29032-29039, 2022.

[17] W. Li, Y. M. Wang, Y. Hei, B. Li, and X. Shi, "A compact low-profile reconfigurable metasurface antenna with polarization and pattern diversities," *IEEE Antennas and Wireless Propagation Letters*, vol. 20, no. 7, pp. 1170-1174, July 2021.

[18] L. Kang, H. Li, B. Tang, X. Wang, and J. Zhou, "Quad-polarization-reconfigurable antenna with a compact and switchable feed," *IEEE Antennas and Wireless Propagation Letters*, vol. 20, no. 4, pp. 548-552, Apr. 2021.

[19] K. Li, Y. Shi, H. Shen, and L. Li, "A characteristic-mode-based polarization-reconfigurable antenna and its array," *IEEE Access*, vol. 6, pp. 64587-64595, 2018.

[20] H. H. Tran, C. D. Bui, N. Nguyen-Trong, and T. K. Nguyen, "A wideband non-uniform metasurface-based circularly polarized reconfigurable antenna," *IEEE Access*, vol. 9, pp. 42325-42332, 2021.

[21] J. Liu, J. Y. Li, J. J. Yang, Y. X. Qi, and R. Xu, "AMC-loaded low-profile circularly polarized reconfigurable antenna array," *IEEE Antennas and Wireless Propagation Letters*, vol. 19, no. 7, pp. 1276-1280, July 2020.

[22] D. Chen, W. Yang, W. Che, Q. Xue, and L. Gu, "Polarization-reconfigurable and frequency-tunable dipole antenna using active AMC structures," *IEEE Access*, vol. 7, pp. 77792-77803, 2019.

[23] C. Ni, M. S. Chen, Z. X. Zhang, and X. L. Wu, "Design of frequency- and polarization-reconfigurable antenna based on the polarization conversion metasurface," *IEEE Antennas and Wireless Propagation Letters,* vol. 17, no. 1, pp. 78-81, Jan. 2018.

[24] H. L. Zhu, S. W. Cheung, X. H. Liu, and T. I. Yuk, "Design of polarization reconfigurable antenna using metasurface," *IEEE Transactions on Antennas and Propagation*, vol. 62, no. 6, pp. 2891-2898, June 2014.

[25] J. Hu, Z.-C. Hao, and W. Hong, "Design of a wideband quad-polarization reconfigurable patch antenna array using a stacked structure," *IEEE Transactions on Antennas and Propagation*, vol. 65, no. 6, pp. 3014-3023, June 2017.

Long Li was born in Guangxi, China, in 1993. He received his B.E. degree in electronic and information engineering from Hohai University, Nanjing, China, in 2017. He received his M.E degree in electronic and communication engineering from South China University of Technology, Guangzhou, China, in 2020. He is now working with the School of Physics and Telecommunication Engineering, Yulin Normal University, Yulin, China. His research interests include reconfigurable antennas, metasurface antennas, and wideband antennas.

Jia-Jun Liang received his B.E. degree in electronic science and technique from Guilin University of Electronic Technology (GUET), Guilin, China, in 2012, and the M.E. degree in radio physics from the University of Electronic Science and Technology of China, Chengdu, China, in 2015. He received the Ph.D. degree in information and communication engineering at Shenzhen University, Shenzhen, China, in 2018. He is now with the School of Physics and Telecommunication Engineering, Yulin Normal University. His current research interests include MIMO antennas, 3D printing antennas, and millimetre wave antennas.

Jier Lv was born in 1964. He received his B.E. degree in physics form Guangxi Normal University, Guilin, China, in 1988. His research interests include nonlinear complex systems and electromagnetic computation.

Xiaoxiao Liu is currently an engineer with Wuhan Maritime Communication Research Insititute. She is mainly engaged in the design of ship antennas, wideband VHF/UHF antennas, reconfigurable antennas, and related technology research.

Tiejun Chen received the B.S. degree from University of Electronic Science and Technology of China, China, in 1988, and received the M.Sc. degree from Guilin University of Electronic Technology, China, in 2007. He is currently a professor in the School of Physics and Telcommunication Engineering, Yulin Normal University, Yulin, China, and he is the senior member of China Electronics Society. His research interests include wireless communications, signal processing, and embedded systems.

Zhao Wu was born in Guangxi, China, in 1987. He received the B.E. degree in electronic and information engineering and the Ph.D. degree in electro-magnetic fields and microwave technology from Xidian University, Xi'an, China, in 2011 and 2016, respectively. From October 2016 to March 2017, he was with Huawei Technologies Co. Ltd. Since April 2017, he has been working with the School of Physics and Telecommunication Engineering, Yulin Normal University. His research interests include metamaterials, novel antennas, reconfigurable antenna design and applications.